ELSEVIER

15 May 1995

OPTICS COMMUNICATIONS

Optics Communications 117 (1995) 198–206

Full length article

Phase locking in a two-element laser array with detuning

Jingwen Xu, K.K. Lee, Y.C. Chen

Department of Physics and Astronomy, Hunter College of the City University of New York, 695 Park Avenue, New York, NY 10021, USA

Received 27 May 1994; revised version received 29 September 1994

Abstract

We have studied the effect of frequency detuning on phase locking in a two-element laser array. The observed modal behavior near the boundary of the locked and unlocked states shows that a two-element laser array can not be characterized simply as a two-mode system. The implication of the new understanding on previous theoretical predictions of laser dynamics is discussed.

1. Introduction

A commonly used method of increasing the output power of semiconductor lasers is the coherent addition of the output of a number of lasers by using evanescent coupling. In the evanescent-coupled semiconductor laser array, a number of laser elements are placed in close proximity to one another so that a small amount of field coupling exists between the nearest neighbors. One- and two-dimensional phase-locked semiconductor laser arrays with a large number of elements have been demonstrated [1,2]. The array geometry has also been used for producing higher power in Nd:YAG and CO_2 lasers. Earlier studies of semiconductor phased arrays are mainly focused on their spatial mode structures under the steady-state operating conditions. These spatial mode patterns in terms of the supermodes have been observed and well understood [3–5]. In a laser array with N elements, the interaction among the elements resulted in the formation of a set of N supermodes, each being a linear superposition of the individual lasing modes. In the case of one-dimensional arrays, the lowest-order supermode corresponds to adjacent elements operating in phase such that the far-field beam pattern is single-lobed centered around zero degree. The highest-order supermode corresponds to adjacent emitters operating 180-degree out of phase such that the center of the intensity distribution in the far field is dark due to destructive interference. Without any modal selection mechanism, the out-of-phase mode usually has the highest modal gain and thus is favored. For obvious reasons, considerable effort has been focused on various techniques to ensure stable operation in the in-phase mode.

Empirical data shows that the lateral distance for phase locking is not more than 10 μm for gain guided semiconductor lasers and 5 μm for index-guided semiconductor lasers [4]. In semiconductor lasers with individually addressable contacts, phase locking has been observed for separations as large as 20 μm [6]. When phase locking is viewed as injection locking through the evanescence waves, the maximum lateral distance to maintain phase locking is set by the requirement that the injected field be much larger than that of the spontaneous emission of the individual elements. Other factors, such as the frequency detuning between individual elements and the cavity Q-value, which affect injection locking are also believed to affect phase locking. So far, there has been no systematic and more controlled experimental study of these phenomena.

In this paper we present an experimental study of phase locking in a two-element laser array with detun-

SSDI 0030-4018(94)00686-5

ing. The study is done in a two-element optically-pumped evanescent-wave coupled Nd:YAG laser array [7,8]. The optically-pumped solid-state laser array is chosen because the key parameters, such as detuning and coupling strength can be accurately controlled and easily varied. The measurements of the dynamical variables are also made easier by much slower time scale of laser dynamics.

2. Experiment

The schematic of the laser array is shown in Fig. 1. Two 808 nm diode lasers are used to end-pump a 5 mm long Nd:YAG etalon, creating two lasing filaments, each operating in the fundamental transverse mode. The diameter of the pumping beams is 50 μm. The separation between the filaments can be continuously varied, without affecting the alignment, by adjusting the positions of the pumping beams. This enables us to study the locking range for various coupling strength. The two end surfaces of the YAG etalon are polished flat and nearly parallel with a four-second wedge angle and are coated with 100% and 95% reflectivity at 1064 nm. The wedge angle provides a detuning between the two-elements. The detuning frequency can be varied by rotating the etalon about the axis of propagation, and can be detected from the beat waves when the two elements are unlocked. The transverse mode of the individual element is mainly determined by the thermally-induced refractive-index waveguide. In Nd:YAG, the refractive-index increase with respect to temperature is about 7×10^{-6}/K [9]. The real part of the refractive-index step, measured from the movement of the beating frequency as a function of the pumping power, is 2×10^{-6} at threshold. The imaginary part of the refractive index step, determined by the modal gain at threshold, is 1.5×10^{-6}. Although the refractive-index profile of the waveguide is expected to be bell shaped, we assume a rectangular profile to simplify the analysis. The calculated fwhm of eigenmode of the stepped index waveguide is in close agreement with the experimentally measured result. The real and imaginary part of the refractive-index profiles are shown in Fig. 2.

When the two elements are phase locked in the anti-symmetric mode, the far-field intensity distribution exhibits a dark fringe at the center. For fixed wedge angle, the detuning increases linearly with separation. As the inter-element separation is increased while keeping a fixed relative wedge angle, the far-field pattern eventually become broad single-lobed which is the incoherent addition of the eigen mode of two incoherent elements. The breaking of phase locking is signified by a beat wave that can be detected by using an RF spectrum analyzer. To generate the map of the boundary of phase-locked region, the inter-element separation is continuously increased for a fixed wedge angle and the frequency of the beat waves as they first occur

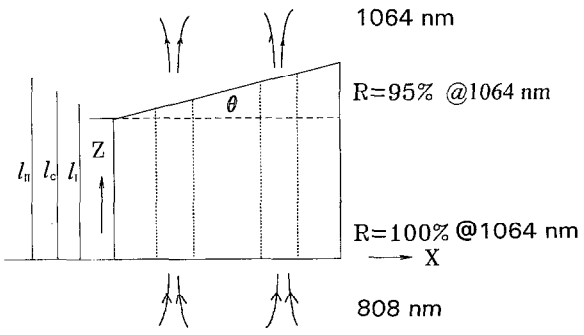

Fig. 1. Schematic of the Nd:YAG etalon with a wedge.

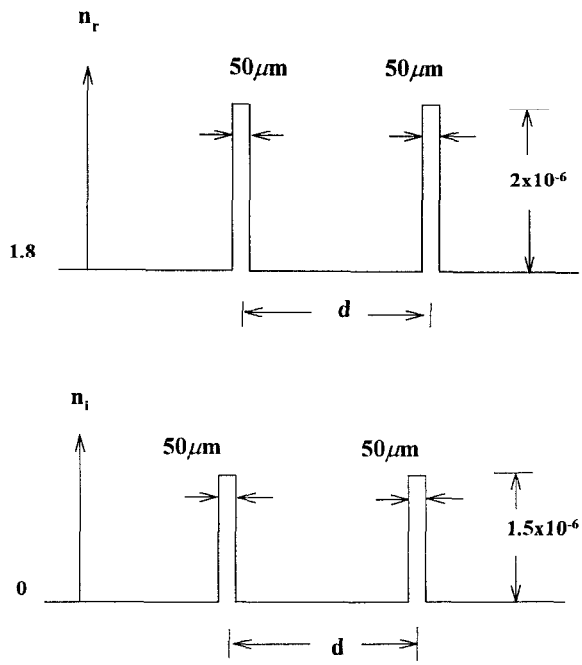

Fig. 2. Real and imaginary refractive-index profiles of the waveguide.

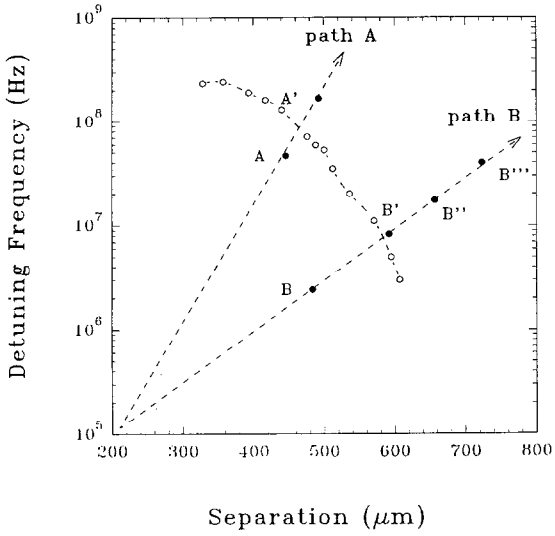

Fig. 3. Measured detuning frequency (open circles) at the boundary of phase locked and unlocked states as a function of inter-element separation. Path A and B are the experimental path along which the separation between the two elements are varied.

is recorded as a function of the separation. The wedge angle is then increased/decreased and the experiment repeated to find the new locking boundary. The data are plotted in Fig. 3 with open circles. The boundary of the beat frequency ranges from 200 MHz for $d = 300$ μm to 2 MHz for $d = 600$ μm. Phase locking is not observed for $d > 600$ μm.

The modal patterns and the transitional behavior in the vicinity of the boundary is worth noting. To observe the far-field patterns cross the boundary the two elements are pulled apart along path A and path B, which corresponding to different wedge angle. Pictures have been taken at various positions along the path, shown as filled circles in Fig. 3. For small inter-element separation and large detuning, the transition from the phase-locked to unlocked states is abrupt as the boundary is crossed along path A in Fig. 3. The occurrence of the beat wave is accompanied by a distinct change in the modal patterns from the two-lobed far-field profile, shown in Fig. 4a, to the single-lobed profile shown in Fig. 4b. For large inter-element separation and small detuning, the transition is gradual and the phenomenon is more complex. The occurrence of the beat wave is accompanied by the reduction of the contrast ratio in the two-lobed far-field, as shown in Figs. 5a and 5b. As the separation is further increased, the patterns undergo an evolution from the two-lobed profile to the three-lobed profile with a peak at the center (Fig. 5c), and, for further increase of separation, to the broad single-lobed profile (Fig. 5d).

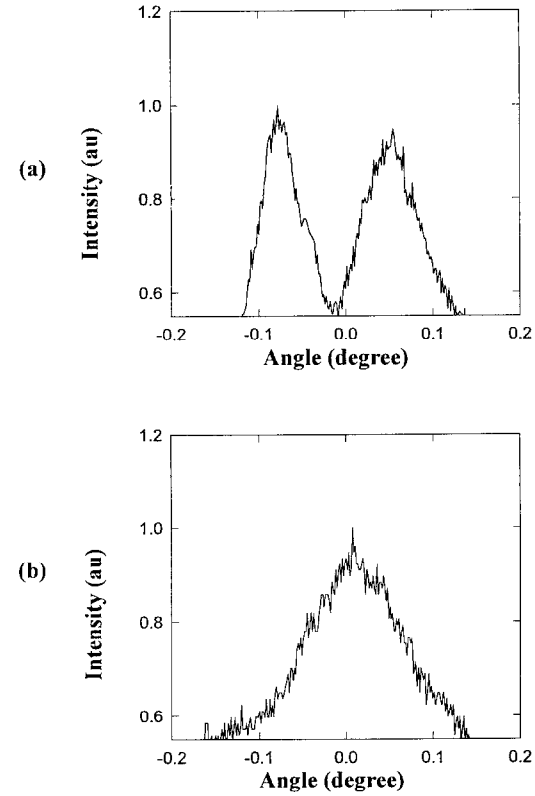

Fig. 4. Observed far-field patterns at various positions (filled circles) along path A, in Fig. 3, measured at points (a) A and (b) A'.

3. Analysis and discussion

In the following, we will show that the observed modal patterns and transitional behavior can be explained based on the competition among the various eigen modes of the composite waveguide. First, we would like to point out that a two-element laser array with detuning is not a two-mode system but can possess numerous eigenmodes at different frequencies. Fig. 6 illustrates the calculated near-field modal intensity patterns representing three different resonance conditions for an etalon with 15 MHz detuning between the elements. The numerical calculation was done using the beam-propagation method [9] in an active waveguide. The laser is treated as an active Fabry–Pérot etalon

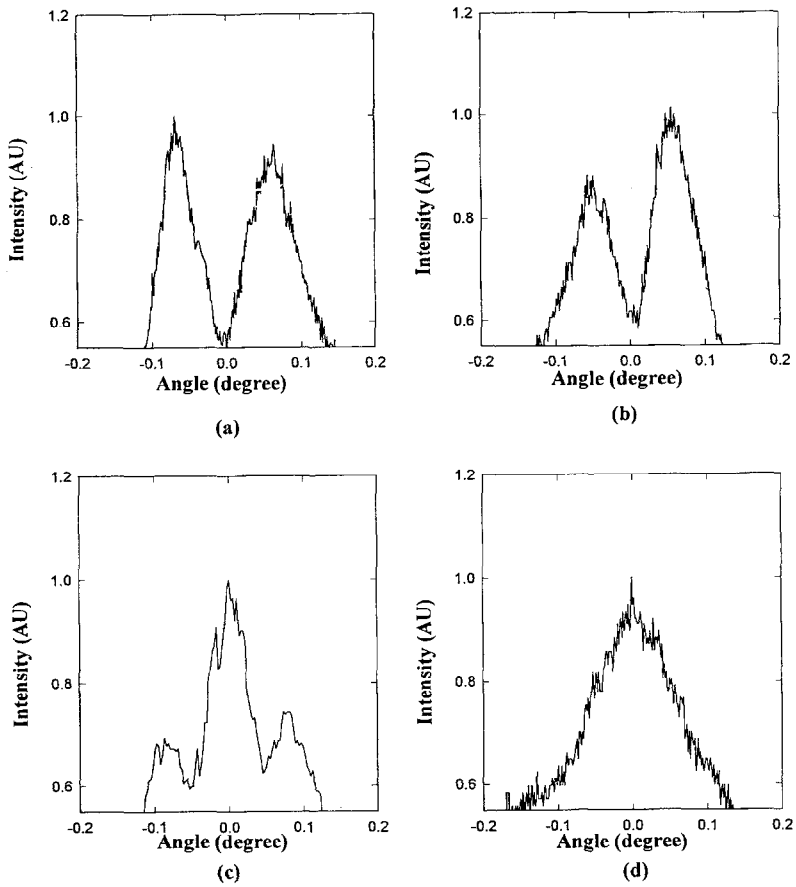

Fig. 5. Observed far-field patterns at various positions (filled circles) along path B, in Fig. 3, measured at points (a) B, (b) B′, (c) B″, and (d) B‴.

whose resonance linewidth is given by the laser linewidth of 200 kHz. For an initial field of arbitrary amplitude and phase distribution, the waves undergo repeated round trips in the cavity. The steady-state field is obtained by integrating the intra-cavity field over the coherence time of 30 μs. For the purpose of later discussion, only the modes with one node are generated for each frequency. The commonly known phase-locked mode, denoted as mode C has a frequency that is resonant with the averaged cavity length $l_c = (l_I + l_{II})/2$ of the composite waveguide. The waves propagating in the two branches of the waveguide in the wedged etalon are slightly off resonance by an equal amount and the resultant fields are equal in magnitude, as shown in Fig. 6b. For any other frequencies, the waves propagating in the two branches of the waveguide experience different interference conditions, resulting in an asymmetric field distribution. Modes I and II in Figs. 6a and 6c correspond to frequencies nearly resonant with the cavity lengths l_I and l_{II}, respectively. If the detuning is sufficiently large, nearly all the intensity of modes I and II resides in one of the element as shown in Fig. 7 for a detuning of 350 MHz. For the detuning frequencies of interest in this paper, the difference in the length of the gain medium in the two branches is less than 10 Å. Thus these two asymmetric modes have nearly the same modal gain and can exist simultaneously, resulting in a beat wave at the detuning frequency.

The lasing mode is the eigen modes of the composite waveguide with the largest modal gain. (The modal gain is the imaginary part of the modal index.) Mode C is favored over Modes I and II if

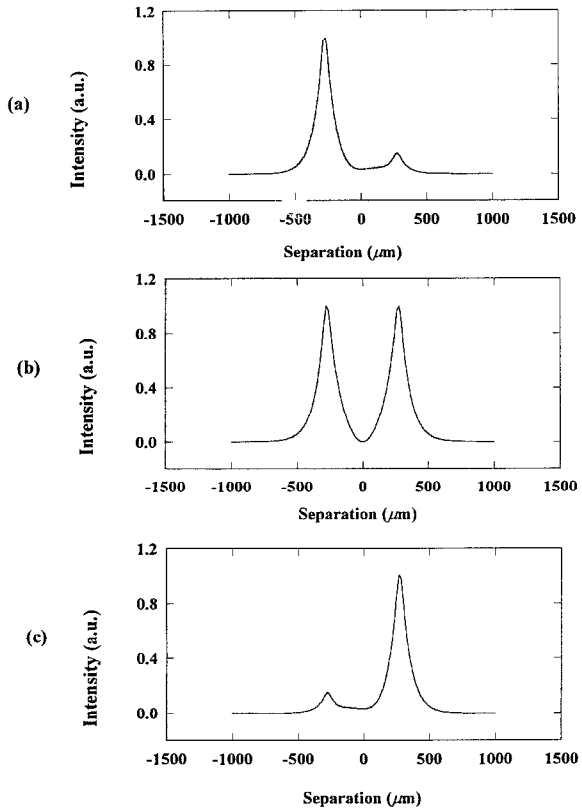

Fig. 6. Calculated near-field patterns for waves resonant with (a) the left branch, (b) the composite waveguide, and (c) the right branch. The inter-element separation of 550 μm and detuning frequency of 15 MHz.

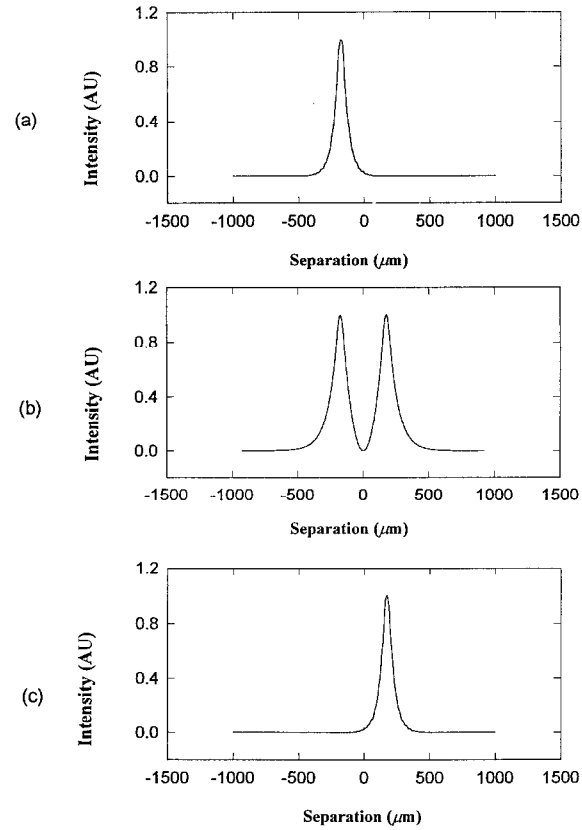

Fig. 7. Calculated near-field patterns for wave resonant with (a) the left branch, (b) the composite waveguide, and (c) the right branch. The inter-element separation is 350 μm and the detuning frequency is 350 MHz.

$$\exp[2g_c(\Delta\omega)l]\ R[1-\alpha_c(\Delta\omega)] > \exp[2g_i(\Delta\omega)l]R[1-\alpha_i(\Delta\omega)]\ , \qquad (1)$$

where g is the modal gain of the waveguide, l is the cavity length, R is the mirror reflectivity, α is the coupling coefficient per reflection at the mirror. Both g and α are functions of the detuning frequency, $\Delta\omega$. For small detuning frequencies, Mode C is favored owing to its higher modal gain. Depending on the detuning frequency at the boundary, two limiting regions are discussed as following.

3.1. Strong coupling

For small inter-element separations, the normalized coupling coefficients can be as large as 0.1. The breaking of phase locking typically occurs at large detuning frequencies involving the type of modes shown in Fig. 7. The abrupt transition is due to the switching from Mode C, shown in Fig. 7b, which gives rise to a two-lobed far-field profile, to Modes I and II, shown in Figs. 7a and 7c, which give rise to a broad single-lobed far-field profiles. In this regime, modal gains of Modes I and II can be approximated by those of the single element laser. The effect of unequal length between the two elements created by the wedge angle of the etalon is to introduce a position-dependent phase shift across the wave front and accompanied loss after each round trip inside the cavity. Assuming that the phase shift occurs near the wedged mirror, the coupling coefficient $\alpha(\Delta\omega)$ upon reflection from the mirror can be calculated from the overlapping integral of the wavefunctions of the incident and reflected waves:

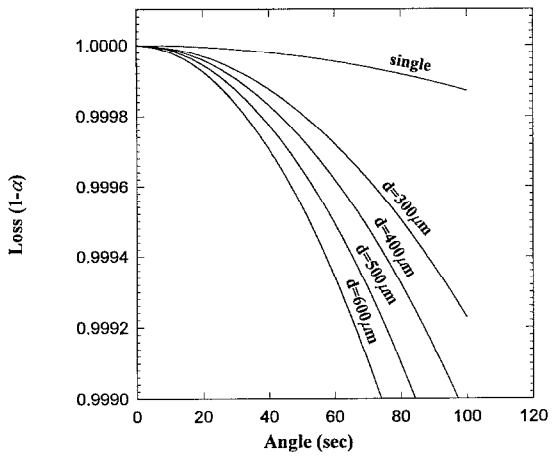

Fig. 8. Calculated coupling coefficient $(1-\alpha)$ as function of wedge angle for various inter-element separations.

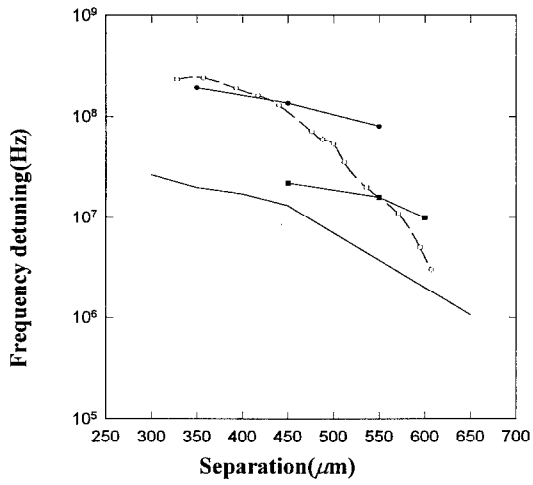

Fig. 9. Calculated detuning frequency for the strong coupling (filled circles) and weak coupling (triangles) regimes for comparison with the experimental data (open circles). The solid curve is calculated using coupled-oscillator equations.

$$\alpha(\Delta\omega) = \left| \int \psi \exp[i2k\Delta z(x)]\ \psi^* \right|^2, \qquad (2)$$

where $z(x) = x \tan\theta$ and θ, the wedge angle, is related to the detuning frequency by $\Delta\omega(\Omega d/l)\tan\theta$ where d is the separation between the two waveguides, Ω is the laser frequency, and l is the cavity length. For a given wedge angle, the coupling loss is larger for a beam with larger effective cross section. Thus the coupling loss, $1-\alpha$, of Mode C increases more rapidly with the wedge angle than those of Modes I and II. The calculated loss, $(1-\alpha)$, as a function of wedge angle for various inter-element separation is shown in Fig. 8. For sufficiently large wedge angle, the difference in the coupling loss can eventually offset the difference in the modal gain. The calculated cross-over points, corresponding to the boundary of the phase locked and unlocked states, are plotted in Fig. 9 by the solid line with filled circles. In this calculation, the wavefunction of mode C is the eigen function of the composite waveguide and those of the mode I and II are approximated by the wavefunctions of the individual waveguide. In the regime of small inter-element separation, the calculated detuning frequencies at the boundary of phase locking are remarkably close to the experimental values for small inter-element separations considering that there is no adjustable parameter in the calculation. The calculated boundary for large inter-element deviates from the experiment because the approximation of the wavefunctions of modes I and II by the wavefunctions of the single element laser is no longer valid. This will be further discussed in the following paragraph.

3.2. Weak coupling

For large inter-element separation, the breaking of phase locking occurs at small detuning frequencies. The mode competition near the boundary involves the type of modes shown in Fig. 6. In the small detuning regime, the loss caused by the wave front tilt at the wedged mirror is negligible. The main effect of increasing detuning is to cause changes in the modal gain due to redistribution of field between the two elements. To calculate the modal gain, the effect of a small detuning frequency in the Fabry–Pérot cavity is assumed to cause a steady-state effective mirror reflectivity, γ, in each branch given by

$$\gamma = \frac{(1-r)^2}{1+r^2-2r\cos(2kd)}, \qquad (3)$$

where d is the cavity length, r is the reflectivity of the output coupler, k is the wave number. The γ factor is 1 for on resonance and is less than 1 for off resonance. The loss $(1-\gamma)$ is then incorporated into the refractive-index profile of the waveguide by adding $\delta n_i = \ln(\gamma)/4\Gamma$ to the imaginary part of the refractive index steps where Γ is the overlapping integral of the modal intensity with the gain medium. The modified

refractive-index profiles are then used for calculating the modal gains. For Mode C, the detuning results in a rapid decrease in the modal gain due to deviation from resonance in both branches. For Modes I and II, the effect of detuning is to shift the intensity toward the element that is closer to resonance, resulting a slower decrease in the modal gains with increasing detuning frequency. The calculated cross-over points are plotted by the solid line with triangles in Fig. 9. This calculation predicts a much smaller tolerance of detuning in closer agreement with the experimental measurement. Furthermore, the features of the modal patterns in the vicinity of the transition can also be explained by this modeling. Fig. 10 shows the calculated near-field and far-field modal patterns of the operating modes when the separation is increased for a given wedge angle. The phase-locked mode has a contrast ratio 1 as shown in Fig. 10a. As the boundary is crossed, the onset of two independent asymmetric modes results in reduced contrast ratio, as shown in Fig. 10b. For larger separation, a three-lobed pattern occurs due to the intensity addition of two modes with highly uneven intensity distribution in the two elements as shown in Fig. 10c. For further increase in separation, a broader single-lobed profile is obtained as shown in Fig. 10d.

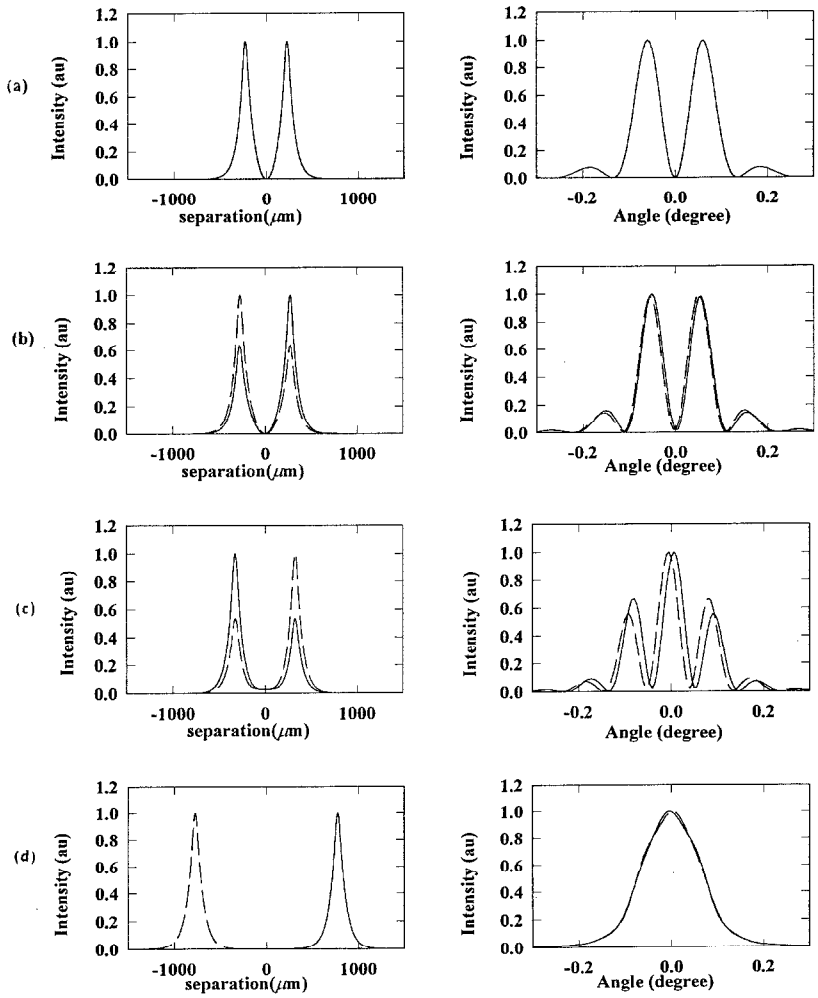

Fig. 10. Calculated modal patterns of near-field and far field of the dominant operating modes for various inter-element separations. The solid and dashed curves represent the eigen modes resonant with one of the elements of the composite waveguide.

In the present experiment, the beat frequency of two unlocked lasers has a short-term fluctuation of 1 MHz over a 1 ms period, corresponding to a relative temperature variation of 3×10^{-4} K. The absence of phase locking for $d>600$ μm can be attributed to the time-varying detuning which is comparable to the detuning tolerance.

Finally, it is illuminating to compare the experimental results with the usual predictions based on the equations for the coupled-oscillators model. The equations for the coupled-oscillators model are

$$\frac{dE_1}{dt} = \frac{g'}{2}(N_1 - N_{th})E_1 + \frac{\kappa_R c}{n}[E_2 \sin(\Delta\phi)] - \frac{\kappa_I c}{n}[E_2 \cos(\Delta\phi)], \quad (4)$$

$$\frac{dE_2}{dt} = \frac{g'}{2}(N_2 - N_{th})E_2 - \frac{\kappa_R c}{n}[E_1 \sin(\Delta\phi)] - \frac{\kappa_I c}{n}[E_1 \cos(\Delta\phi)], \quad (5)$$

$$\frac{d(\Delta\phi)}{dt} = \Delta\omega + \frac{k_R c}{n}\left(\frac{E_2}{E_1} - \frac{E_1}{E_2}\right)\cos(\Delta\phi) + \frac{k_I c}{n}\left(\frac{E_2}{E_1} + \frac{E_1}{E_2}\right)\sin(\Delta\phi), \quad (6)$$

$$\frac{dN_1}{dt} = P - \frac{N_1}{\tau_s} - \left(\frac{1}{\tau_p} + g'(N_1 - N_{th})\right)E_1^2, \quad (7)$$

$$\frac{dN_2}{dt} = P - \frac{N_2}{\tau_s} - \left(\frac{1}{\tau_p} + g'(N_2 - N_{th})\right)E_2^2, \quad (8)$$

where N_i is the population inversion and E_i is the field amplitude of the individual lasers, and $\Delta\phi$ is the phase difference of the two lasers. The other parameters are the differential gain g', the photon lifetime τ_p, the complex coupling coefficient $\kappa = \eta n/c\tau_p$, the threshold population inversion N_{th}, the pump rate P, the lifetime of the excited state τ_p, and the frequency detuning $\Delta\omega$. The parameters used are $\tau_s = 200$ μs, $\tau_p = 1.2$ ns, $g'N_{th} = 5.13\times10^9$/s, $P = 1.3P_0$. For an initial field of arbitrary amplitudes and relative phase and a given detuning frequency, the system is considered phase locked if, after periods of transient oscillations, the amplitude and the relative phase reach a steady state. The system is considered unlocked if the relative phase increases linearly with time, creating a beating phenomenon of two independently operating lasers. The locking range and locking dynamics are strongly influenced by the magnitude of η_i and to a much less degree by η_r. If η_i is neglected, the calculated boundary of phase locking for our experimental condition is five orders of magnitude smaller than the experimental values. In the vicinity of the boundary, there also exists a region in which the laser amplitude and phase exhibit irregular oscillations. If η_i is set to be $\Delta g/2g$ where Δg is the difference of the numerically calculated modal gains of the symmetric and antisymmetric supermodes, the calculated boundary of stable phase-locking, ranging from 23 MHz for $\eta_i = 0.1023$ at $d = 300$ μm to 3 MHz for $\eta_i = 0.03$ at $d = 600$ μm, plotted the solid curve in Fig. 9. Thus the calculated detuning frequencies of stable phase locking is one order of magnitude smaller than the experimental values. Furthermore, the coupled-oscillators equations predict eigen modes with nearly equal intensity distribution in the two branches and can not account for the observed complex modal behavior in the transition region.

Our study shows that the breaking of the "phase-locked" mode is due to the onset of two independently operating sets of eigenmodes of the composite waveguide at different frequencies. The system can not be characterized simply as a coupled two-oscillator system. The complex modal behavior in the vicinity of the boundary of phase locking also can not be synthesized simply by the coupled two-oscillator equations. This finding has a profound implication on the predictions of temporal instability based on the coupled-oscillator equations. The temporal instability as predicted by coupled rate equations can result in a temporal variation in the modal gains of the launched field to become either higher or lower than the steady state value. When the modal gain is momentarily lower than the steady state value, the onset of more favorable modes, which are not eigen modes of the coupled-oscillator equations with different frequencies, whose profile overlaps better with the gain profile can overpower the nonlinear dynamics predicted based on the deterministic model.

Acknowledgements

This project is supported by New York State Center for Advanced Technology (CAT) on Ultrafast Photonic Materials and Applications at the City University

of New York, by Ballistic Missile Defense Organization grant N00014-94-1-0865 and by a CUNY Faculty Research Award.

References

[1] D. Scifres, R. Burnham and W. Streifer, Appl. Phys. Lett. 33 (1978) 1015.
[2] S. Sanders, R. Waarts, D. Nam, D. Welch, D. Scifries, J.C. Ehlert, W.J. Cassarly, J.M. Finlan and K.M. Folld, Appl. Phys. Lett. 64 (1994) 1478.
[3] T.L. Paoli, W. Streifer and R.D. Burnham, Appl. Phys. Lett. 45 (1984) 217.
[4] D. Botez and J. Connolly, Appl. Phys. Lett. 43 (1983) 1096.
[5] E. Kapon, J. Katz and A. Yariv, Optics Lett. 10 (1984) 125.
[6] E. Kapon, C. Lindsey, J. Katz, S. Margalit and A. Yariv, Appl. Phys. Lett. 44 (1984) 389.
[7] Jingwen Xu, S. Li, K.K. Lee and Y.C. Chen, Conference of Quantum Electronics and Laser Sciences (1993) paper QWF4.
[8] Jingwen Xu, Shiqun Li, K.K. Lee and Y.C. Chen, Optics Lett. 18 (1993) 513.
[9] W. Koechner, Solid State Laser Engineering (Springer, Berlin, 1992) p. 51.
[10] A.G. Fox and T. Li, IEEE J. Quantum Electron. QE-4 (1968) 460.
[11] G.P. Agraw and N.K. Dutta, Long wavelength semiconductor lasers, 1st Ed. (Van Nostrand Reinhold, 1986).
[12] A.G. Fox and T. Li, Bell Sys. Tech. J. 40 (1961) 453.
[13] K. Otsuka, Phys. Rev. Lett. 65 (1990) 329.
[14] S.S. Wang and H.G. Winful, Appl. Phys. Lett. 52 (1988) 1774.